Supplemental figures and legends

Figure S1

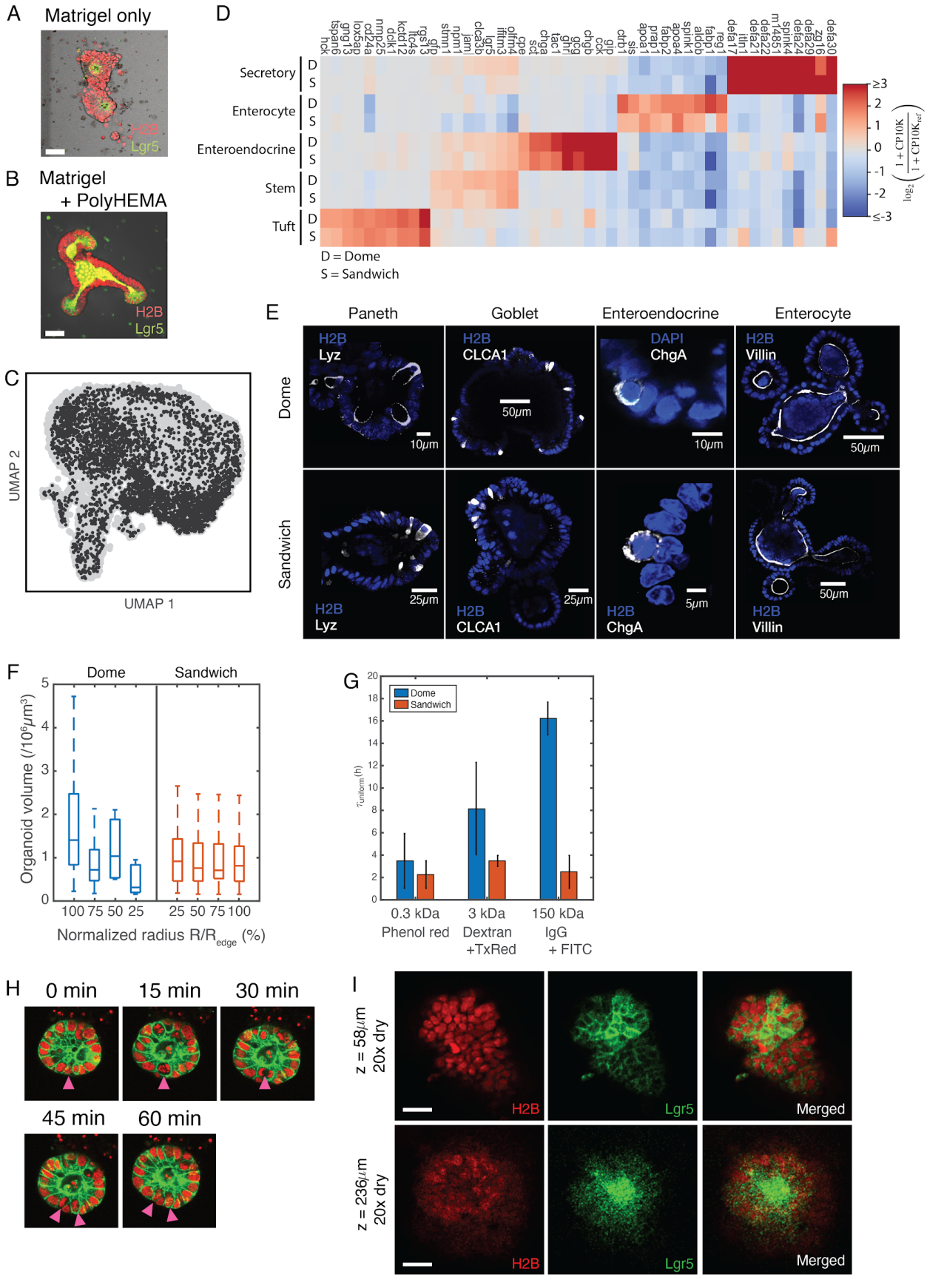

Figure S1 (supporting Fig. 1). Characterization of triple-decker hydrogel sandwich cultures.
(A) In Matrigel-only sandwiches (Lee et al., 2007), intestinal organoids penetrate the base layer and spread out onto the underlying coverslip. Scale bar: 50 μm.
(B) In a Matrigel sandwich atop a glass coverslip pre-coated with PolyHEMA, organoids show normal three-dimensional morphology after 9 days in culture. Scale bar: 50 μm.
(C) UMAP embedding of scRNA-seq data (13,062 cells x 30,005 genes) from dome and sandwich (n=6 wells each) cultures, as in **Fig. 1C**. Gray = all cells; black = sandwich culture cells.
(D) Comparison of marker genes in scRNA-Seq data, for major epithelial cell types between cells grown in dome and sandwich cultures. Values show log-scaled mean expression in transcriptomes classified to each of the cell types, normalized to the median mean value for each gene.
(E) Immunofluorescence detection of cell type markers shows conservation of cell types in organoids grown in dome and sandwich cultures.
(F) Distributions of organoid volumes at different distances from the center of each culture well (n = 3 wells per condition), showing that organoid growth is more spatially uniform in triple-decker sandwiches (right) than in Matrigel domes (left).
(G) The time for diffusible molecules to distribute uniformly in Matrigel is considerably shorter in sandwich cultures than in dome cultures. The time τ_{uniform} indicates the time required for the concentration of a fluorescently-labeled molecule to equilibrate between the center and edge of the base of a dome (blue) and a triple-decker sandwich (orange). With $I_{\mathrm{center,edge}}$ being the recorded fluorescent intensities at the radial center and edge of the Matrigel, respectively, then $\tau_{\mathrm{uniform}} = \min_t I_{\mathrm{center}} \geq 0.8 I_{\mathrm{edge}}$. n = 3 replicates per fluorescently-labeled molecule per culture condition.
(H) Mitotic tracking at 40X magnification; magenta arrows show a dividing cell and its progeny. Scale bar: 10 μm.
(I) An organoid in a triple-decker sandwich imaged using standard 0.75 NA 20x dry objective (top); the same optics yield noticeably degraded images of organoids located further from the coverslip in dome culture (bottom). Scale bar: 40 μm.

Figure S2

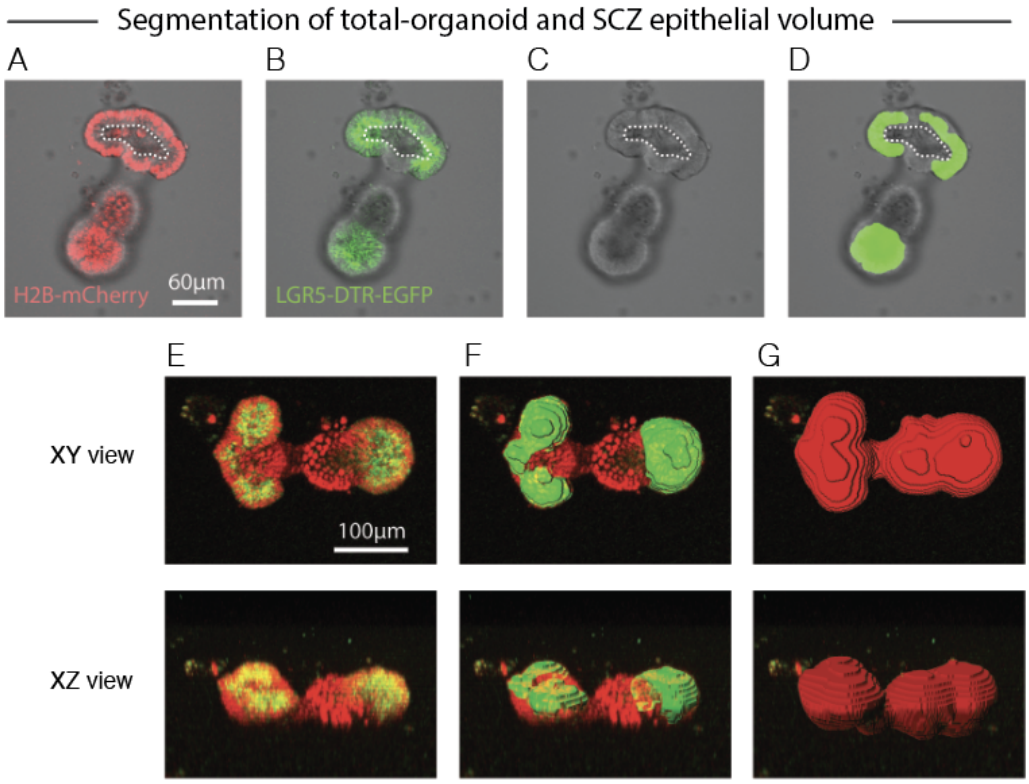
Segmentation of total-organoid and SCZ epithelial volume
A
B
C
D
H2B-mCherry
60µm
LGR5-DTR-EGFP
E
F
G
XY view
100µm
XZ view

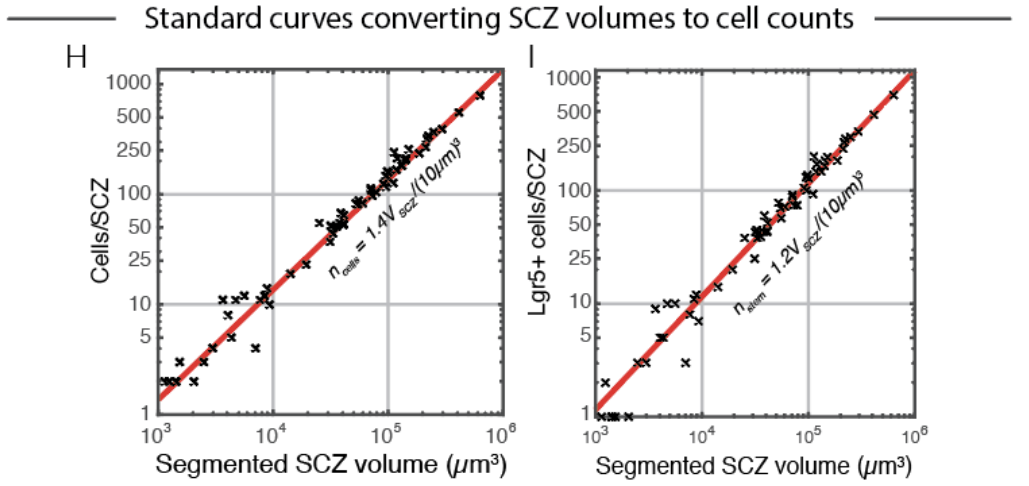
Standard curves converting SCZ volumes to cell counts
H
Cells/SCZ
$n_{cells} = 1.4V_{SCZ}/(10\mu m)^3$
Segmented SCZ volume (µm³)
I
Lgr5+ cells/SCZ
$n_{stem} = 1.2V_{SCZ}/(10\mu m)^3$
Segmented SCZ volume (µm³)

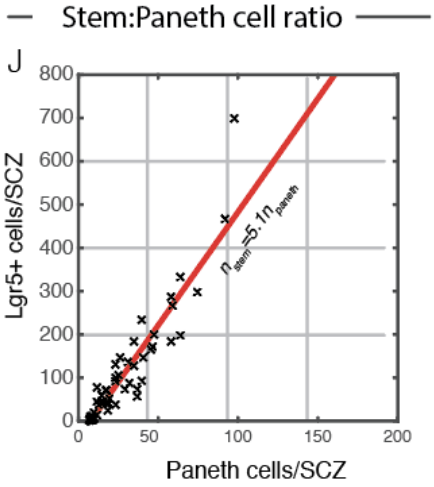
Stem:Paneth cell ratio
J
Lgr5+ cells/SCZ
$n_{stem}=5.1n_{paneth}$
Paneth cells/SCZ

Figure S2 (supporting Fig. 2). Segmentation of SCZ and whole organoid size.
(A-D) Micrographs showing steps in SCZ segmentation (see Methods for all steps of pipeline): a single optical section of (A) H2B-mCherry, (B) Lgr5-DTR-EGFP, or (C) bright-field image only, showing the boundaries of the organoid lumen (dashed line) and (D) the segmented SCZ region of the cross-section. Representative of n = 659 SCZs segmented to generate Figs. 2E,J.
(E-G) Volumetric rendering of the same organoid, showing (E) the raw image, (F) the segmented volumes of SCZs, and (G) the segmented volume of the whole organoid.
(H,I) Comparison of cell numbers manually counted in n = 61 SCZs to segmented SCZ volumes. The low noise and linearity of these curves supports the segmentation approach. The trendline provides a standard curve relating segmented SCZ volume to cell numbers reported in **Fig. 2E,J**.
(J) Ratio of Paneth cells to Lgr5+ cells in SCZs remains approximately constant across organoid sizes.

Figure S3

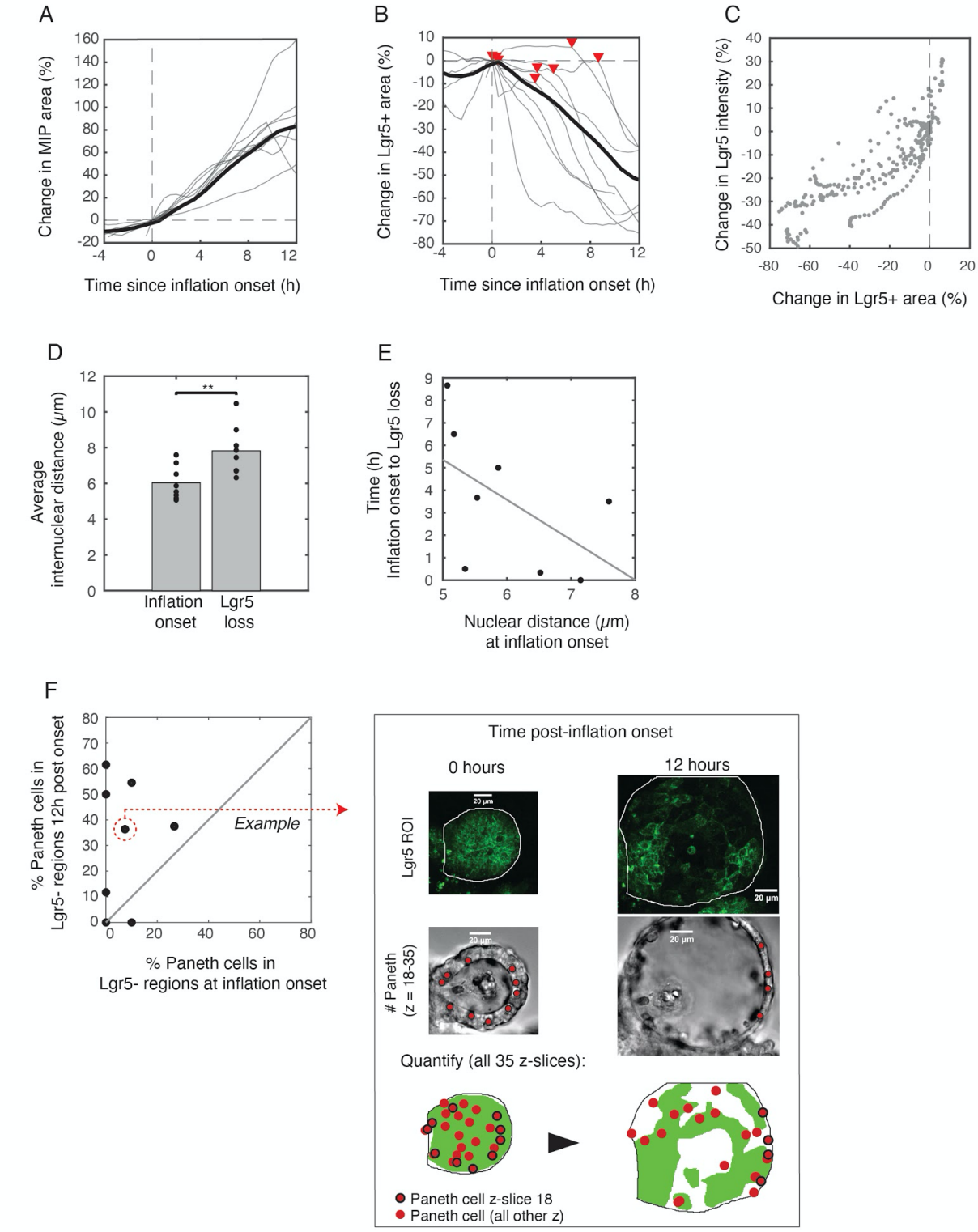
A
Change in MIP area (%)
Time since inflation onset (h)
B
Change in Lgr5+ area (%)
Time since inflation onset (h)
C
Change in Lgr5 intensity (%)
Change in Lgr5+ area (%)
D
Average internuclear distance (μm)
**
Inflation onset
Lgr5 loss
E
Time (h) Inflation onset to Lgr5 loss
Nuclear distance (μm) at inflation onset
F
% Paneth cells in Lgr5- regions 12h post onset
Example
% Paneth cells in Lgr5- regions at inflation onset
Time post-inflation onset
0 hours
12 hours
Lgr5 ROI
Paneth (z = 18-35)
20 μm
Quantify (all 35 z-slices):
Paneth cell z-slice 18
Paneth cell (all other z)

Figure S3 (Supporting Fig. 4). Lgr5 loss occurs after inflation onset and epithelial stretch can override Paneth cell niche factors.

(A-C) Analysis of timing of Lgr5 loss during bud inflation. (A) In silico synchronization of bud inflation, by quantifying the projected cross-sectional area using maximum intensity projections (n=8 movies analyzed). Percentage changes relative to inflation onset (t = 0) are shown. (B) In silico synchronized traces of the %Lgr5+ area in maximum intensity projections, showing loss of Lgr5 after the onset of inflation. Arrows indicate the onset time (*T*) of Lgr5 loss, which was identified by fitting the curves to a piecewise-linear model *%LGR5 = {b for t<T; b-a*(t-T) for t>T}*. (C) Control plot showing consistency in quantifying Lgr5 based on total integrated intensity or %Lgr5+ epithelium. Both approaches to quantifying Lgr5 signal show consistent Lgr5 loss (bottom left quadrant).

(D) Average inter-nuclear distance of Lgr5+ cells in buds in the n=8 movies analyzed. The distance is compared between the start of inflation and the (variable) time at which Lgr5 loss initiates, indicated by the red triangles in panel (B) above.

(E) The time between inflation onset and the onset of Lgr5 loss (see panel B) inversely correlates with inter-nuclear distance at inflation onset.

(F) The fraction of Paneth cells lacking contact with Lgr5+ cells in each bud at inflation onset, and at 12 hours after inflation onset. In 6/8 observations, this fraction increases after inflation onset, indicating that Lgr5+ cells can lose Lgr5 expression as they stretch even if they neighbor Paneth cells.

Figure S4

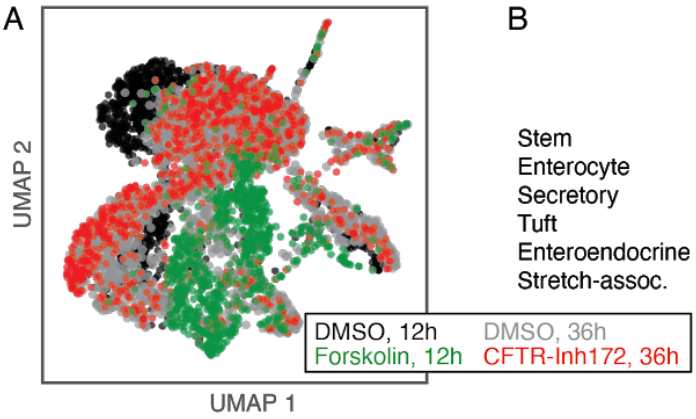

B

p-values for change in population fractions (6B)

			Bonferroni-corrected	
	Forskolin	CFTR-inh	Forskolin	CFTR-inh
Stem	$1.4x10^{-15}$	0.28	$1.7x10^{-14}$	1
Enterocyte	$2.4x10^{-6}$	0.14	$2.9x10^{-5}$	0.14
Secretory	0.15	$4.4x10^{-4}$	1	$5.3x10^{-3}$
Tuft	0.13	0.08	1	0.96
Enteroendocrine	0.58	0.13	1	1
Stretch-assoc.	$5.0x10^{-5}$	$3.8x10^{-4}$	$6.0x10^{-4}$	$4.6x10^{-3}$

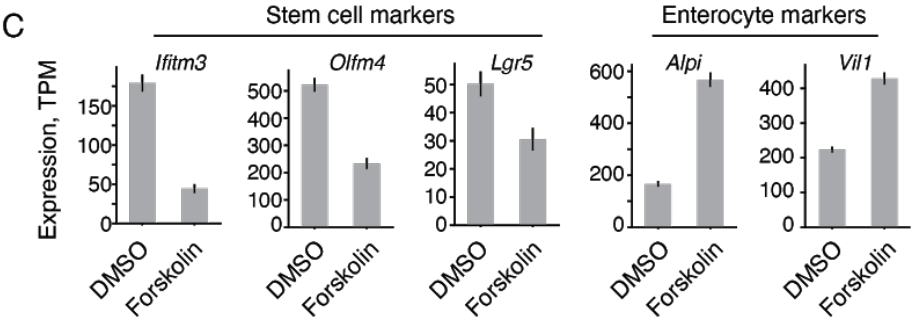

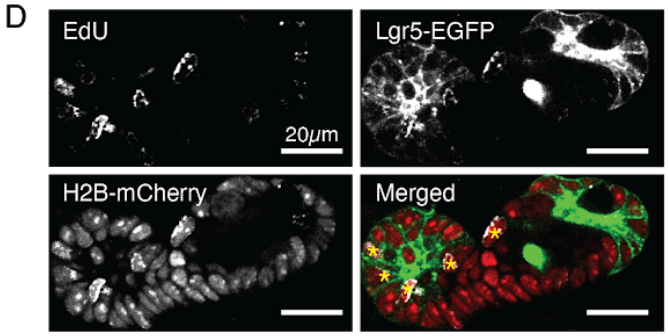

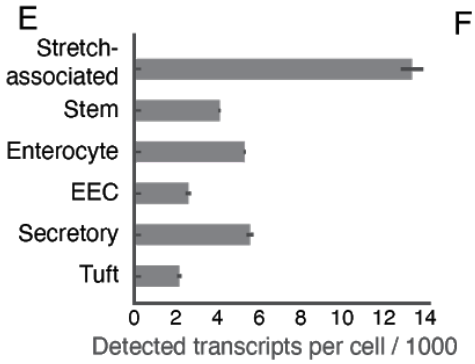

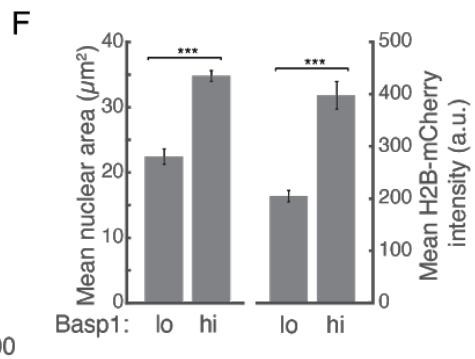

Figure S4 (Supporting Fig. 6). Single cell RNA-Seq analysis of organoids under CFTR channel stimulation and inhibition
(A) UMAP representation of scRNA-Seq data (5,241 cells x 29,603 genes; n=10 wells total) as in **Fig. 6A**, colored by condition.
(B) Table of p-values for changes in population abundance for annotated cell states. Fisher Exact tests are used, with comparison of time-matched DMSO to treated samples.
(C) Mean expression of selected markers of stem cells and mature enterocytes over all cells analyzed by scRNA-Seq after 12 forskolin or vehicle (DMSO). Changes are consistent with the observed increase in the fraction of enterocytes and reduction in stem cells after treatment (see **Fig. 6B**).
(D) Representative image of an organoid incubated for 2 hours with EdU to detect cells in S phase after 36 hours of treatment with CFTRinh-172, Ouabain, or DMSO. Quantitative analysis of %EdU positive cells across organoids is shown in **Fig. 6D**.
(E) Total detected transcript counts across annotated states, showing an increased size of stretch-associated cells. Error bars = SEM.
(F) Mean nuclear area and mean nuclear intensity of H2B-mCherry in Basp1-high cells (n = 31), compared to adjacent Basp1-low cells (n = 31), recapitulates scRNA-Seq in panel (E).